Real-fluid effects of primary methanol fuel on dual-fuel injection and mixing

Hesham Gaballa, Chaouki Habchi, Jean-Charles de Hemptinne

ILASS-Americas 32nd Annual Conference on Liquid Atomization and Spray Systems, May 22-25, 2022

Real-fluid effects of primary methanol fuel on dual-fuel injection and mixing

H. Gaballa*, C. Habchi*, and J.C. De Hemptinne
IFP Energies nouvelles, Institut Carnot IFPEN Transports Energie,
1 et 4 avenue de Bois-Préau, 92852 Rueil-Malmaison, France

Abstract

The reduction of greenhouse gases (GHG) emitted into the earth's atmosphere, such as carbon dioxide, has obviously become a priority. Replacing the majority of fossil fuels with cleaner renewable fuels (such as methanol) in dual-fuel internal combustion engines for heavy-duty vehicles is one proposed solution to reduce GHG emissions. This paper aims to study the fuel injection and mixing in such a dual-fuel configuration, where the ambient environment is a mixture of primary fuel (methanol) and nitrogen. For this investigation, the Engine Combustion Network (ECN) Spray A condition is used as a reference. Large-eddy simulations (LES) are performed using a two-phase multi-component real-fluid model (RFM) closed by a thermodynamic equilibrium tabulation approach. The proposed tabulation approach can further handle ternary mixtures in contrast to previous research limited to binary mixtures. Thermodynamic tables are generated using the in-house IFPEN-Carnot thermodynamic library based on vapor-liquid equilibrium calculations coupled with different real-fluid equations of state. The thermodynamic closure of the two-phase model is achieved using a tabulated Peng-Robinson (PR) and Cubic Plus Association (CPA) equations of state for the single and dual-fuel cases, respectively. Detailed analysis of the dual-fuel configuration versus its single-fuel counterpart is discussed based on the LES results and the implemented real-fluid thermodynamics. The LES predictions match well with the ECN experimental database for the single-fuel case. In the dual-fuel configuration, liquid and vapor penetrations and fuel radial distribution are revealed to exhibit minimal variations compared to the single-fuel case. The thermodynamic analysis demonstrates that evaporation and mixing occur following a different thermodynamic path in the dual-fuel case, but with minimal variation in the two-phase region with respect to the single-fuel case, leading to relatively similar behavior. The dual-fuel case also showed a higher level of dissolved ambient gas in the liquid jet than the single-fuel case.

*Corresponding Author: chawki.habchi@ifpen.fr, hesham.gaballa@ifpen.fr

Introduction

Dual-fuel internal combustion engine (DFICE) is one of the promising concepts to reduce the pollutant emissions from diesel-powered heavy-duty vehicles. In dual-fuel engines, a primary fuel is premixed with air in the intake, then drawn into the cylinder, and during the compression stroke, a small quantity of pilot diesel fuel is injected to ignite the premixed primary fuel-air mixture [1]. A review of the different primary fuel injection strategies in dual fuel engines can be found in [2]. Various fuels have been investigated as primary fuels in DFICE, such as methane, short-chain alcohols (methanol and ethanol), hydrogen, and ammonia.

Several experimental studies [3, 4] have demonstrated the potential of employing short-chain alcohols such as methanol and ethanol as primary fuels in DFICE to reduce the soot and nitrogen oxides (NOx) emissions. These fuels offer several advantages, including being renewable, lower cost, and produced from biomass, or Carbon dioxide and hydrogen. Despite the aforementioned advantages, the effective design of the fuel injection equipment for DFICE is a challenging task and a key priority for the further development of these engines.

To this goal, fuel injection and mixing need to be further understood under dual-fuel configuration due to its direct impact on combustion efficiency and resultant emissions. In the current work, the evaporation and mixing of the Engine Combustion Network (ECN) spray A [5] under a dual-fuel configuration is investigated using a newly developed real-fluid modeling approach. Methanol is exclusively employed as a primary fuel in the current study.

Dual-fuel combustion has been the subject of various numerical [6, 7, 8] and experimental [9, 10, 4] studies mainly focusing on investigating the effect of the primary fuel on the combustion process as well as soot and emissions production. The numerical studies mainly relied on the Discrete Droplet Model (DDM) [11] approach for modeling the fuel injection. In this approach, the liquid phase is described by Lagrangian particles/blobs, whereas the gas-phase is modeled in an Eulerian framework. However, It has been shown that this approach inherent various shortcomings [12], especially in the near nozzle region, where the primary break-up initiates from the intact liquid core [13]. Indeed, the accurate modeling of the spray injection and atomization is an essential step for the following combustion phase [14].

Accordingly, the current work is focused on modeling the dual-fuel spray injection, evaporation, and mixing using an Eulerian-Eulerian (E-E) diffused interface two-phase flow model. The employed real-fluid model (RFM) [15, 16, 17] is closed by a thermodynamic equilibrium tabulation approach. A thermodynamic table is generated before the CFD simulation based on a vapor-liquid equilibrium (VLE) calculation coupled to a real-fluid equation of state (EoS). The adopted tabulation approach is one remedy to the direct evaluation of the costly phase-equilibrium solver during the CFD simulation, especially when coupled with a complex real-fluid EoS [18, 19]. The thermodynamic model considers the different thermodynamic regimes that may coexist during the fuel injection event. Indeed, both subcritical and supercritical states may exist simultaneously based on the local pressure, temperature, and species composition compared to the mixture's critical point, as demonstrated in [17, 18, 20].

Several contributions to spray injection modeling using an E-E two-phase flow models closed by tabulated real-fluid thermodynamics have been reported in the literature. A tabulated thermodynamic approach based on the PC-SAFT EoS has been proposed by Koukouvinis et al. [21] and applied to the ECN spray A injection simulation. Besides, Jafari et al. [17] proposed an efficient tabulation approach to investigate the cryogenic injection of liquid nitrogen co-axially injected with hot hydrogen jet into supercritical nitrogen. Albeit the contribution provided by the previously mentioned work, It was limited to binary mixtures tabulation. Thereby, further development of a tabulation approach capable of handling ternary mixtures as those encountered in dual-fuel engines is indeed required.

To this goal, the current work proposes a real-fluid thermodynamic tabulation approach for ternary mixtures [15] relevant to dual-fuel engines. More precisely, a thermodynamic table is generated for ternary mixtures using the in-house IFPEN-Carnot thermodynamic library and coupled to the CONVERGE CFD solver [22]. The proposed model is used to investigate the evaporation and mixing of fuel injection under the ECN spray A condition in a dual-fuel configuration. The current investigation is carried out in two steps. In the first step, the RFM model is validated against the ECN spray A experimental database for single fuel (SF) configuration. Then, in the following step, the effect of introducing methanol in the ambient gas relevant to dual-fuel (DF) configuration is investigated.

The main objectives of the current study are: first, to propose a predictive model for multi-species two-phase flow simulations with phase change without the need of tuning sub-models coefficients as in classical Lagrangian spray models. Second, to answer the question "What is the effect of methanol

used as a primary fuel in the dual-fuel configuration on the evaporation and mixing processes?". The performed analysis is based on Large-Eddy Simulations (LES) using the proposed RFM model closed by tabulated real-fluid thermodynamics for the (n-dodecane/nitrogen) binary mixture in the SF case and the (n-dodecane/nitrogen/methanol) ternary mixture in the DF case.

The current paper is organized as follows: Section 2 describes the RFM model, including the transport equations and the thermodynamic tabulation approach. Section 3 first presents the test case setup, followed by the RFM model validation against the ECN experiments for the SF case. Then, n-dodecane injection in a mixed (methanol and nitrogen) ambient relevant to DF configuration is discussed under the ECN spray A condition. Finally, Section 4 summarizes the main conclusions of the current study.

Real-fluid model (RFM) description

Governing equations

The diffused interface two-phase flow model adopted in the current study is a four equation model that is fully compressible and considers multi-component in both phases under the assumptions of thermal and mechanical equilibrium. The filtered set of governing equations (1-4) expresses the conservation of mixture mass, mixture momentum, mixture total energy, and species mass fraction, respectively.

$$\frac{\partial \bar{\rho}}{\partial t} + \frac{\partial \bar{\rho}\tilde{u}_i}{\partial x_i} = 0 \tag{1}$$

$$\frac{\partial \bar{\rho}\tilde{u}_i}{\partial t} + \frac{\partial \bar{\rho}\tilde{u}_i\tilde{u}_j}{\partial x_j} = -\frac{\partial \bar{P}}{\partial x_i} + \frac{\partial}{\partial x_j}(\bar{\tau}_{ij} + \bar{\tau}_{ij}^{sgs}) \tag{2}$$

$$\begin{aligned}\frac{\partial \bar{\rho}\tilde{e}}{\partial t} + \frac{\partial \bar{\rho}\tilde{u}_j\tilde{e}}{\partial x_j} =& -\bar{P}\frac{\partial \tilde{u}_j}{\partial x_j} + (\bar{\tau}_{ij} + \bar{\tau}_{ij}^{sgs})\frac{\partial \tilde{u}_i}{\partial x_j} + \\ & \frac{\partial}{\partial x_j}(\bar{Q}_j + \bar{Q}_j^{sgs})\end{aligned} \tag{3}$$

$$\frac{\partial \bar{\rho}\tilde{Y}_k}{\partial t} + \frac{\partial \bar{\rho}\tilde{u}_j\tilde{Y}_k}{\partial x_j} = \frac{\partial}{\partial x_j}(\bar{J}_{k,j} + \bar{J}_{k,j}^{sgs}) \tag{4}$$

where (ρ, u_i, P, e) are the mixture's density, velocity, pressure, and specific internal energy, respectively. The viscous stress tensor (τ_{ij}) is expressed as $(\tau_{ij} = \mu(\partial u_i/\partial x_j + \partial u_j/\partial x_i) - \frac{2}{3}\mu(\partial u_k/\partial x_k\delta_{ij})$, where (μ) is the dynamic viscosity and δ_{ij} is the Kronecker delta. The heat flux (Q_j) is defined as $(Q_j = \lambda\frac{\partial T}{\partial x_j} + \rho\sum_k D_k h_k \frac{\partial Y_k}{\partial x_j})$, where (T) is the mixture's temperature, (λ) is the thermal conductivity, and (D_k, h_k, Y_k) are the mass diffusion coefficient, specific enthalpy, and mass fraction of species k, respectively. The (λ) and (μ) are computed by Chung et al. [23] correlations. The species diffusion flux $(J_{k,j})$ is defined as $(J_{k,j} = \rho D_k \frac{\partial Y_k}{\partial x_j})$. The LES subgrid-scale terms denoted by the superscript (sgs) in the governing equations are modeled. The subgrid stress tensor (τ_{ij}^{sgs}) is computed similarly to (τ_{ij}), with the eddy viscosity assumption, replacing the molecular viscosity with the subgrid-scale viscosity (μ_{sgs}) computed by the Sigma model [24]. The subgrid species $(J_{k,j}^{sgs})$ and heat (Q_j^{sgs}) fluxes are modeled using the gradient assumption, where the molecular transport coefficients in $(J_{k,j})$ and (Q_j) are replaced with the turbulent ones. The turbulent transport coefficients are modeled by introducing turbulent Schmidt number $(Sc_t = 0.7)$ and turbulent Prandtl number $(Pr_t = 0.9)$. The turbulent mass diffusion coefficient is computed as $(D_t = \mu_{sgs}/\rho Sc_t)$ and the turbulent conductivity is computed as $(\lambda_t = C_p\mu_{sgs}/Pr_t)$, where (C_p) is the isobaric heat capacity.

Tabulated thermodynamic closure

The fully compressible multi-component two-phase flow system described above is closed by a tabulated real-fluid EoS adopting a local thermodynamic equilibrium hypothesis. To consider the phase change phenomenon, the EoS is not sufficient, but a VLE calculation is also included in this study. The current work proposes a pre-tabulation approach, where before the CFD simulation, a thermodynamic table is generated for binary [16, 17] or ternary [15] mixtures using the IFPEN-Carnot thermodynamic library. The thermodynamic library performs the VLE calculation using a robust isothermal-isobaric (TP) flash [25] coupled to a real-fluid EoS. The tabulated properties include the thermodynamic equilibrium density, internal energy, fluid-phase state and composition, and necessary thermodynamic derivatives as heat capacity, sound speed, and transport properties. The thermodynamic table inputs are the temperature (T), pressure (P), and species mass fraction $(Y_k, k = 1, N_s - 1,$ where N_s is the total number of species). Thus, the tables are three-dimensional (3D) for binary systems and four-dimensional (4D) for ternary systems. During the simulation, required tabulated quantities are interpolated using the inverse distance weighting method (IDW) [26]. The thermodynamic table is coupled with CONVERGE CFD solver [22] as detailed in [15, 16, 17]. The thermodynamic table is used during the simulation for two main tasks as follow:

- Properties look-up: compute the thermodynamic and transport properties, phase state, and composition from $(T, P, Y_k, k = 1, N_s - 1)$ obtained by the flow solver.

- Temperature reverse look-up: compute the temperature from the $(e, P, Y_k, k = 1, N_s - 1)$ provided by the flow solver.

The tabulated thermodynamic closure is achieved using the Peng-Robinson (PR) [27] EoS for the (n-dodecane /nitrogen) binary system in the single-fuel spray A simulation. For the dual-fuel simulation, the Cubic Plus Association (CPA) [28] EoS is employed for the (n-dodecane/nitrogen/methanol) ternary system. Compared to PR-EoS, the CPA EoS with its additional association term can be efficiently used to model mixtures including hydrocarbons and polar compounds (methanol) [29]. Volume translation [30] has been used to improve the accuracy of the liquid phase density predicted by the PR and CPA EoSs.

Results and discussion

The current study is based on the ECN spray A test case, where liquid n-dodecane ($C_{12}H_{26}$) is injected into gaseous nitrogen (N_2) at the conditions listed in Table 1. Firstly, the RFM model is validated against the available experimental database for the spray A single-fuel case. Then, the same test case is investigated in a dual-fuel configuration, by introducing methanol in the ambient gas so that the chamber includes initially a mixture of nitrogen and methanol.

Fuel	n-dodecane
Injection pressure (MPa)	150
Injection temperature (K)	363
Ambient temperature (K)	900
Ambient pressure (MPa)	6
Ambient density (kg/m^3)	22.8
Ambient composition	Pure N_2

Table 1: Injection and ambient conditions of ECN spray A

Test case setup

The employed numerical setup comprises a rectangular chamber, which is 20 mm in the stream-wise direction and 10 mm in the lateral directions. The nozzle outlet diameter is 0.0894 mm corresponding to spray A injector serial #210675 [31]. The grid structure is depicted in Fig. 1, where the base grid size is 400 µm located at the outer edge of the domain, while several mesh refinement levels have been employed to achieve a minimum cell size of ~ 6 µm in the first 3mm from the nozzle exit. Thus, the nozzle outlet diameter is discretized with about 15 cells. The total mesh count is around 3M cells.

The injection conditions are applied at the domain inlet by an inlet boundary condition (BC), based on a time-dependent mass-flow rate profile obtained from CMT virtual injection rate generator [32], which allows to partially reproduce the in-nozzle flow and the needle motion effects [33, 34]. Thus, the injector internal flow was not simulated. It is worth noting that inlet BC is set without imposing any synthetic turbulent fluctuations. A no-slip boundary condition is applied at the wall around the nozzle outlet (on left side of the chamber). All the rest of the domain boundaries are outlets with a pressure boundary condition of 6 MPa.

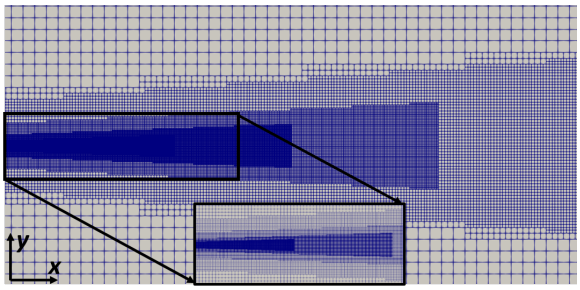

Figure 1: Computational domain with the grid structure at the central cut section. The insert shows a zoom of the refined mesh in the near-nozzle exit region.

LES simulations are carried out using the RFM model described above. The numerical solution of the transport equations (1-4) is based on a modified Pressure Implicit with Splitting of Operator (PISO) algorithm [35] for the pressure-velocity coupling. The spatial discretization is second-order accurate using a central difference scheme. The time integration is achieved by a second-order Crank-Nicolson scheme for the momentum equation and a first-order implicit Euler scheme for the rest of the equations. The time step is around 2-3ns and adjusted automatically based on a maximum acoustic Courant number of 0.5.

Spray A single fuel (SF)

A qualitative comparison of the n-dodecane jet temporal evolution between the LES results and the experimental data (diffused back illumination) [36] is depicted in Fig. 2. The blue iso-line superimposed on the LES n-dodecane mixture fraction field demonstrates the liquid penetration with a liquid volume fraction ($LVF = 0.15\%$).

The simulation results show a qualitatively good agreement with the experimental data with similar

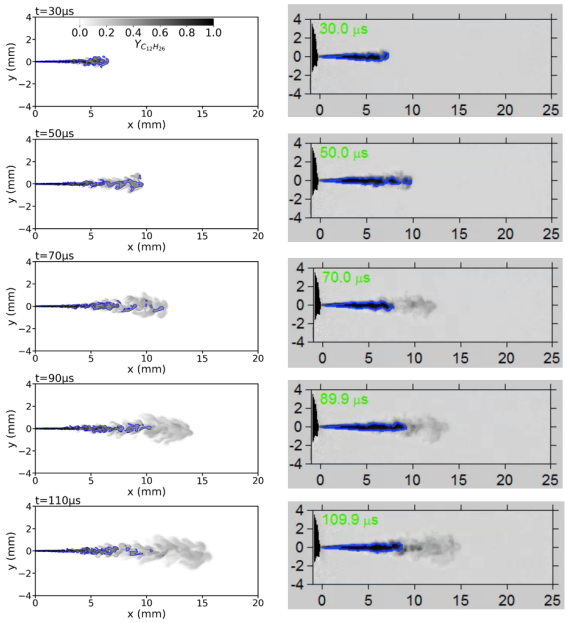

Figure 2: Temporal evolution of the n-dodecane injection. left column: LES results; right column: experimental data [36]. Instantaneous n-dodecane mixture fraction distribution is presented for the LES results. The blue line superimposed on the LES results represents a LVF iso-line of 0.15%, which illustrates the liquid penetration length.

penetrations for both liquid and vapor.

A quantitative comparison of the spray penetrations between the LES results and the experiments is shown in Fig. 3. The experimental results correspond to the vapor penetration from the #210677 injector [37] and liquid penetration from the #210675 injector [36]. In the LES, the liquid penetration length is defined as $\max(x(LVF = 0.15\%))$, where (x) is the axial distance from the nozzle exit. The criterion to evaluate the liquid penetration length is based on the Mie-scattering theory analysis [38], where the LVF threshold value representing the liquid length was found to be $(LVF < 0.15\%)$ at spray A conditions. The vapor penetration length is defined as $\max(x(Y_{C_{12}H_{26}} = 0.1\%))$ as recommended by ECN [39], where $(Y_{C_{12}H_{26}})$ is the dodecane mass fraction. It can be seen that the LES results are in good agreement with the experimental liquid and vapor penetrations. The vapor penetration tends to be slightly overestimated at $t = 0.16$ ms, when the liquid jet becomes diluted close to the end of the computational domain ($x = 20$ mm) in areas of relatively coarse resolution.

In addition, a comparison of the radial dis-

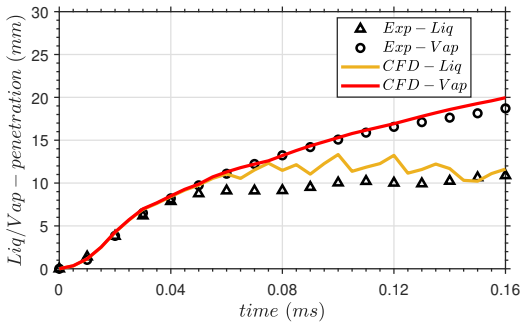

Figure 3: liquid jet vapor and liquid penetrations. CFD stands for LES simulation results. Exp-Vap corresponds to vapor penetration data from #210677 injector [37] and Exp-liquid to liquid penetration from diffused back-illumination (DBI) of the #210675 injector [36].

tribution of n-dodecane mass fraction between the LES results and experiments is depicted in Fig. 4. The presented numerical result is obtained by time-averaging the LES results in the time interval between 0.4 and 1 ms after the start of injection (during the quasi-steady period). The error bars of the experimental results are presented using 95% of confidence level [40].

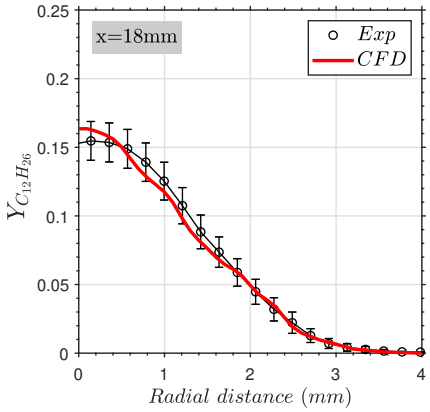

Figure 4: Comparison of the time averaged LES results of n-dodecane mass fraction radial distribution against the experimental results [40] at an axial distance of 18 mm from the nozzle exit.

The obtained numerical results shows a good agreement with the experimental data within its confidence level. The peak value on the jet axis tends to be slightly overestimated. However, the spray decay along the radial direction is well repro-

duced compared to the experimental profile.

To further analyze the phase change and mixing processes, the temperature-composition phase diagram for n-dodecane-nitrogen mixture at (P = 6 MPa) together with the adiabatic mixing temperature (T_{AM}) is shown in Fig. 5. The (T_{AM}) is formulated as,

$$h_{mix}(T_{AM}, P_{amb}) = Y_{C_{12}H_{26}}\, h_{C_{12}H_{26}}(T_{C_{12}H_{26}}, P_{amb}) + Y_{amb}\, h_{amb}(T_{amb}, P_{amb}) \quad (5)$$

where h, $Y_{C_{12}H_{26}}$, Y_{amb} are the specific enthalpy, the n-dodecane, and the ambient gas mass fractions, respectively. $T_{C_{12}H_{26}}$, T_{amb}, P_{amb} denote the initial temperature of the fuel (n-dodecane), the initial temperature of the ambient, and the ambient pressure, respectively. For the single-fuel case ($Y_{amb} = Y_{N_2}$), since the ambient includes only pure nitrogen. The adiabatic mixing temperature is computed considering the phase change based on the VLE solver. The scattered data on Fig. 5 represents the thermodynamic states obtained from the LES simulation at $t = 110$ µs.

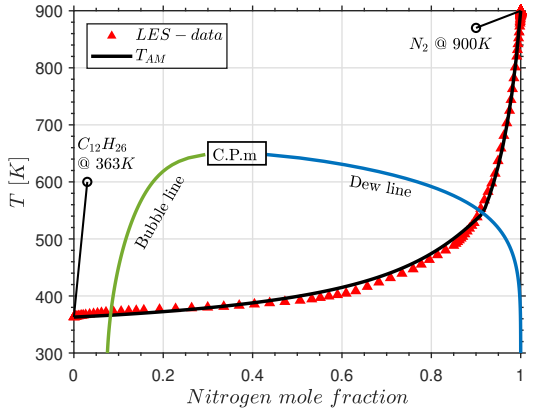

Figure 5: Temperature-composition diagram of ($C_{12}H_{26} - N_2$) binary mixture at pressure of 6 MPa along with the adiabatic mixing temperature (T_{AM}) obtained from the VLE solver. Scattered data denote the thermodynamic states from the LES simulation at $t = 110$ µs.

It can be seen that the mixture temperature distribution from the LES can follow well the adiabatic mixing temperature in almost all the N_2 concentration range. Besides, it shows that the temperature distribution has crossed the two-phase region bounded by the bubble and dew lines. This confirms that subcritical phase transition occurs for the ($C_{12}H_{26} - N_2$) binary mixture even at a pressure of 6 MPa higher than the pure n-dodecane critical pressure (P_{cr} = 1.8 MPa), as also demonstrated in previous studies [20, 18].

The previous comparison of the numerical results with the experiments shows that the RFM model employed in the current work can accurately represent the jet evaporation and mixing. Thus, it can be further applied with sufficient confidence to investigate the spray evaporation and mixing in the dual-fuel configuration.

Spray A dual-fuel (DF)

For the dual-fuel investigation, the same numerical setup and operating condition of the single-fuel spray A are employed. The main difference is that the chamber is initialized with a mixed ambient of methanol (CH_3OH) and nitrogen (N_2) with mass fractions of 0.2 and 0.8, respectively. Besides, the thermodynamic closure is obtained using a tabulated CPA EoS. The employed initial mass fraction of methanol (Y_{CH_3OH} = 0.2) could be relatively higher than that found in dual-fuel engines powered with methanol. However, the goal here is to investigate if significant effects on the evaporation and mixing could take place even with such initial methanol ambient concentration.

Figure 6 shows a comparison of the spray liquid and vapor penetrations between the single-fuel (SF) and dual-fuel (DF) cases.

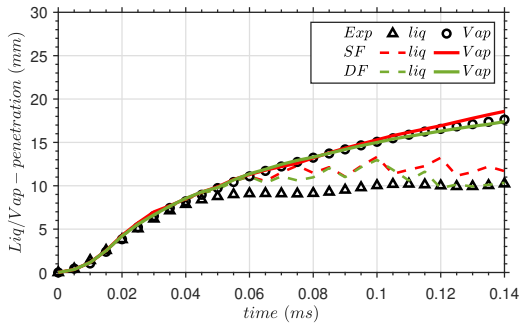

Figure 6: Comparison of jet liquid and vapor penetrations between spray A single-fuel (SF) and dual-fuel (DF) cases. The ambient of the DF case is composed of 20% methanol and 80% nitrogen by mass fraction

It can be seen that the initial presence of methanol in the ambient gas has a minimal effect, on the spray liquid and vapor penetration, when comparing the SF and DF cases.

In addition, the time-averaged n-dodecane mass fraction radial distribution is compared between the

SF and DF cases as depicted in Fig. 7. The SF and DF cases show a highly similar radial fuel distribution with a slightly narrower profile at the jet periphery for the DF case.

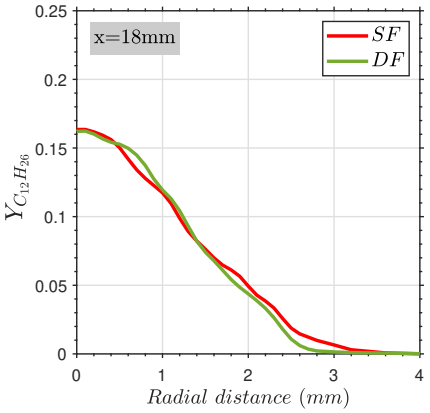

Figure 7: Comparison of the time averaged simulation results of n-dodecane mass fraction radial distribution between single-fuel (SF) and dual-fuel (DF) cases at an axial distance of 18 mm from the nozzle exit.

To further understand the fundamental origin of such behavior of the DF case compared to the SF reference case, Fig. 8 shows the adiabatic mixing temperature variation with the n-dodecane mole fraction for the SF and DF cases. The adiabatic mixing temperature is obtained from the VLE solver. The two-phase states along the adiabatic mixing temperature line are colored blue for both cases. For the dual-fuel case, the ambient is a mixture of nitrogen and methanol with mass fractions of 0.8 and 0.2, respectively. Thus, the (Y_{amb}) term in Eq. 5 is formulated as ($Y_{amb} = Y_{CH_3OH} + Y_{N_2}$), with $Y_{CH_3OH} = 0.2\,Y_{amb}$ and $Y_{N_2} = 0.8\,Y_{amb}$.

It can be observed that the adiabatic mixing temperature is relatively higher for the DF case than the SF case. Besides, the two-phase region shrinks slightly for the DF case compared to the SF case, as demonstrated by the insert on Fig. 8. This minimal variation of the two-phase region between the SF and DF cases explains the similar evaporation and mixing behavior for the two cases as observed in the spray penetrations and fuel radial distribution.

Moreover, the insert on Fig. 8 shows a smaller n-dodecane mole fraction at the start of the two-phase region for the DF case compared to the SF case. This implies that a higher amount of ambient gases is dissolved in the liquid phase for the DF case, relatively to the SF case.

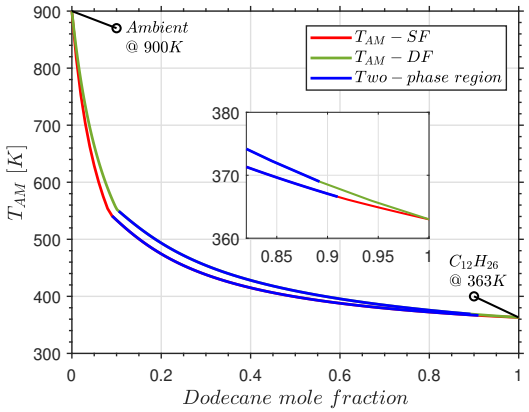

Figure 8: Adiabatic mixing temperature (T_{AM}) along with the two-phase region represented by the blue lines for the SF and DF cases at pressure of 6 MPa.

Figure 9 shows the mass fraction of the dissolved ambient gases ($Y_{amb,liq}$) in the liquid phase at $t = 110$ µs. For the single-fuel case, the dissolved gas includes only nitrogen, whereas, for the dual-fuel case, the dissolved gas is the sum of dissolved methanol and nitrogen in the liquid phase.

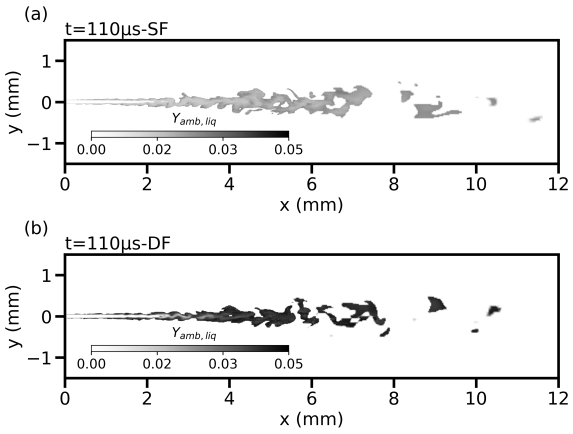

Figure 9: Instantaneous mass fraction of dissolved ambient gases in the liquid phase ($Y_{amb,liq}$) for (a) single fuel (SF) case and (b) dual-fuel (DF) case at $t = 110$ µs. For dual-fuel case, the dissolved gas is the sum of dissolved methanol and nitrogen.

It can be observed that the dissolved gas for the DF case is relatively higher than that of the SF case. These results are consistent with the two-phase region shrink in the insert on Fig. 8, which shows a smaller mole fraction of n-dodecane at the start of

the two-phase region for the DF case (i.e., a higher amount of dissolved gas in the liquid phase).

In addition, the methanol introduced in the chamber also impacts the ambient density. Indeed, the ambient gas density exhibits a relative increase as methanol is added to nitrogen in the chamber, since methanol is a heavier compound than nitrogen. For instance, the ambient gas density (ρ_{amb}) as computed by the CPA EoS increases from ($22\,\mathrm{kg/m^3}$) for the SF case to ($22.6\,\mathrm{kg/m^3}$) for the DF case with methanol mass fraction of 0.2. However, this slight increase in the ambient density did not significantly affect the jet behavior.

Conclusion

To face the current environmental problem, we investigated in this article the feasibility of using methanol to replace the majority of the fossil fuel responsible for greenhouse gases emissions in diesel internal combustion engines.

For this aim, a two-phase real-fluid model (RFM) [15, 16, 17] closed by a thermodynamic tabulation approach has been developed and implemented within CONVERGE CFD solver. The proposed model can further handle ternary mixtures in contrast to previous research limited to binary mixtures tabulation. The required thermodynamic and transport properties are tabulated using the in-house IFPEN-Carnot thermodynamic library based on vapor-liquid equilibrium (VLE) calculations coupled with an appropriate equation of state.

The RFM model has been applied to investigate the injection, evaporation, and mixing of the ECN spray A under single and dual-fuel configurations. In the first step, the ECN spray A is computed in a single fuel (SF) configuration, where the fuel (n-dodecane) is injected into pure nitrogen. The comparison with the ECN experimental data has shown satisfactory agreement for the spray liquid and vapor penetrations and the fuel radial distribution. In addition, the performed thermodynamic analysis has shown that classical subcritical phase transition takes place during the injection event under the considered transcritical condition. Thereby, considering the VLE theory is essential for modeling such conditions.

Next, the ECN spray A is computed in a dual-fuel (DF) configuration by introducing methanol as a primary fuel mixed with nitrogen in the chamber ambient. The obtained results for the DF case have shown similar behavior compared to the SF case. Indeed, minimal deviations have been observed on the spray liquid and vapor penetrations and fuel radial distribution between the single and dual-fuel cases.

The performed thermodynamic analysis has shown that the two-phase region along the adiabatic mixing temperature lines shrinks slightly for the DF case compared to the SF case. However, this slight shrink did not significantly affect the evaporation and mixing processes, leading to similar behavior with the SF case. Besides, it has been found that the n-dodecane mole fraction at the start of the two-phase region along the adiabatic mixing temperature line for the DF case is relatively smaller than that of the SF case. Thus, more ambient gases are dissolved in the liquid phase for the DF case than the SF case. This was also observed in the LES simulations, showing higher levels of dissolved gases for the DF case than the SF case. Additionally, introducing methanol in the ambient gas leads to a relative increase in the ambient density. However, this increase is relatively small, having a negligible effect on the jet behavior.

Although, under the considered dual-fuel configuration, it has been found that the ambient methanol effects on the overall spray evaporation and mixing processes are not significant. However, a remarkable impact on pollutant emissions is to be expected. For instance, a lower NOx formation rate in the dual-fuel configuration with methanol as primary fuel has been demonstrated in [6] under the operating conditions of Spray A.

Finally, the proposed RFM model closed by the real-fluid thermodynamic tabulation approach for ternary mixtures shows great potential for the computation of multi-component two-phase mixtures problems with phase change, avoiding the direct evaluation of costly VLE solver during the simulation run-time.

Acknowledgment

This project has received funding from the European Union Horizon 2020 Research and Innovation programme. Grant Agreement no. 861002 for the EDEM project.

References

[1] L. Wei and P. Geng. *Fuel Processing Technology*, 142:264–278, 2016.

[2] Ghazi A. Karim. *Dual-fuel diesel engines*. CRC Press, 2015.

[3] Le. Ning, Q. Duan, Z. Chen, H. Kou, B. Liu, Bo. Yang, and Ke. Zeng. *Fuel*, 266:117034, 2020.

[4] V.B. Pedrozo, I. May, W. Guan, and H. Zhao. *Fuel*, 230:440–451, 2018.

[5] Engine Combustion Network (ECN), available at. https://ecn.sandia.gov/.

[6] S. Xu, S. Zhong, K. Pang, S. Yu, M. Jangi, and X.-S. Bai. *Applied Energy*, 279:115774, 2020.

[7] B. Tekgül, H. Kahila, O. Kaario, and V. Vuorinen. *Combustion and Flame*, 215:51–65, 2020.

[8] S. Frankl, S. Gleis, S. Karmann, M. Prager, and G. Wachtmeister. *International Journal of Engine Research*, 22(10):3196–3208, 2021.

[9] Y. Dong, O. Kaario, G. Hassan, O. Ranta, M. Larmi, and B. Johansson. *Fuel*, 277:117932, 2020.

[10] S. Gleis, S. Frankl, D. Waligorski, M. Prager, and G. Wachtmeister. *SAE Technical Paper Series*. Warrendale, PA, United States, 2019.

[11] J. K. Dukowicz. *Journal of Computational Physics*, 35(2):229–253, 1980.

[12] Q. Xue, M. Battistoni, C. F. Powell, D. E. Longman, S. P. Quan, E. Pomraning, P. K. Senecal, D. P. Schmidt, and S. Som. *International Journal of Multiphase Flow*, 70:77–88, 2015.

[13] C. Habchi, J. Bohbot, A. Schmid, and K. Herrmann. *Journal of Physics: Conference Series*, 656:012084, 2015.

[14] B. M. Devassy, C. Habchi, and E. Daniel. *Atomization and Sprays*, 25(1):47–80, 2015.

[15] H. Gaballa, S. Jafari, C. Habchi, and J.-C. de Hemptinne. *International Journal of Heat and Mass Transfer*, 189:122671, 2022.

[16] S. Jafari, H. Gaballa, C. Habchi, J.-C. de Hemptinne, and P. Mougin. *The Journal of Supercritical Fluids*, p. 105557, 2022.

[17] S. Jafari, H. Gaballa, C. Habchi, and J.-C. de Hemptinne. *Energies*, 14(18):5621, 2021.

[18] S. Yang, P. Yi, and C. Habchi. *International Journal of Multiphase Flow*, 122:103145, 2020.

[19] P. Yi, S. Yang, C. Habchi, and R. Lugo. *Physics of Fluids*, 31(2):026102, 2019.

[20] J. Matheis and S. Hickel. *International Journal of Multiphase Flow*, 99:294–311, 2018.

[21] P. Koukouvinis, A. Vidal-Roncero, C. Rodriguez, M. Gavaises, and L. Pickett. *Fuel*, 275:117871, 2020.

[22] K.J. Richards, P.K. Senecal, and E. Pomraning. CONVERGE 3.0, Convergent Science, Madison, WI (2021).

[23] T.H. Chung, M. Ajlan, L.L Lee, and K. E. Starling. *Industrial & Engineering Chemistry Research*, 27(4):671–679, 1988.

[24] F. Nicoud, H. B. Toda, O. Cabrit, S. Bose, and J. Lee. *Physics of Fluids*, 23(8):085106, 2011.

[25] M. L. Michelsen. *Fluid Phase Equilibria*, 9(1):21–40, 1982.

[26] C. Ware, W. Knight, and D. Wells. *Computers & Geosciences*, 17(7):985–993, 1991.

[27] D.-Y. Peng and D.B. Robinson. *Industrial & Engineering Chemistry Fundamentals*, 15(1):59–64, 1976.

[28] G. M. Kontogeorgis, E. C. Voutsas, I. V. Yakoumis, and D. P. Tassios. *Industrial & Engineering Chemistry Research*, 35(11):4310–4318, 1996.

[29] J. C. de Hemptine, P. Mougin, A. Barreau, L. Ruffine, S. Tamouza, and R. Inchekel. *Oil & Gas Science and Technology - Revue de l'IFP*, 61(3):363–386, 2006.

[30] A. Péneloux, E. Rauzy, and R. Fréze. *Fluid Phase Equilibria*, 8(1):7–23, 1982.

[31] Engine Combustion Network (ECN), Spray A geometry, available at. http://ecn.sandia.gov/diesel-spray-combustion/target-condition/spray-a-nozzle-geometry.

[32] CMT, Virtual Injection Rate Generator, available at. https://www.cmt.upv.es/#/ecn.

[33] J. M. Garcia-Oliver, J. M. Pastor, A. Pandal, N. Trask, E. Baldwin, and D. P. Schmidt. *Atomization and Sprays*, 23(1):71–95, 2013.

[34] J. M. Desantes, J. M. García-Oliver, J. M. Pastor, A. Pandal, E. Baldwin, and D. P. Schmidt. *International Journal of Multiphase Flow*, 80:89–99, 2016.

[35] R.I Issa. *Journal of Computational Physics*, 62(1):40–65, 1986.

[36] Engine Combustion Network (ECN), Measurements of the liquid length for nozzle 210675 using diffused back-illumination (DBI) at Spray A and other conditions, available at. https://ecn.sandia.gov/data/dbi675/.

[37] Engine Combustion Network (ECN), vapor penetration data from #210677 injector, available at. https://ecn.sandia.gov/cvdata/assets/datafiles/.

[38] Pickett, L. M., Genzale, C. L., Manin, J., Malbec, L., and Hermant, L. ILASS, 2011.

[39] Engine Combustion Network, Modeling Standards and Recommendations, available at. https://ecn.sandia.gov/diesel-spray-combustion/computational-method/modeling-standards/.

[40] Engine Combustion Network (ECN), Rayleigh scattering n-dodecane/ambient mixing images for Spray A and several other experimental conditions, available at. https://ecn.sandia.gov/data/ bkldaal4mixing/.